JBC Papers in Press. Published on December 27, 2019 as Manuscript RA119.009807
The latest version is at http://www.jbc.org/cgi/doi/10.1074/jbc.RA119.009807

Loss of the disease-associated glycosyltransferase Galnt3 alters Muc10 glycosylation and the composition of the oral microbiome

Gabriella Peluso[1], E Tian[1], Loreto Abusleme[2,3], Takashi Munemasa[4,5], Taro Mukaibo[4,5], and Kelly G. Ten Hagen[1,]

From the [1]Developmental Glycobiology Section, National Institute of Dental and Craniofacial Research, National Institutes of Health, Bethesda, Maryland 20892-4370
[2]Laboratory of Oral Microbiology, and [3]Laboratory of Craniofacial Translational Research, Faculty of Dentistry, University of Chile, Santiago, Chile
[4]Secretory Mechanisms and Dysfunctions Section, National Institute of Dental and Craniofacial Research, National Institutes of Health, Bethesda, MD 20892, USA
[5]Division of Oral Reconstruction and Rehabilitation, Kyushu Dental University, Kitakyushu, Fukuoka 803-8580, Japan

Running title: *Galnt3 influences the microbiome*

*To whom correspondence should be addressed: Kelly G. Ten Hagen, Ph.D., Building 30, Room 407, 30 Convent Drive, MSC 4370, Bethesda, MD 20892-4370; Kelly.Tenhagen@nih.gov ;
Tel: 301-451-6318; Fax: 301-402-0897.

Keywords: Galnt3, microbiome, Muc10, mucins, O-glycosylation, hyperphosphatemic familial tumoral calcinosis (HFTC), salivary protein, glycan, post-translational modification, submandibular gland, saliva

ABSTRACT

The importance of the microbiome in health and its disruption in disease is continuing to be elucidated. However, the multitude of host and environmental factors that influence the microbiome are still largely unknown. Here, we examined polypeptide N-acetylgalactosaminyltransferae 3 (*Galnt3*)-deficient mice, which serve as a model for the disease hyperphosphatemic familial tumoral calcinosis (HFTC). In HFTC, loss of GALNT3 activity in the bone is thought to lead to altered glycosylation of the phosphate-regulating hormone fibroblast growth factor 23 (FGF23), resulting in hyperphosphatemia and subdermal calcified tumors. However, GALNT3 is expressed in other tissues in addition to bone, suggesting that systemic loss could result in other pathologies. Using semi-quantitative real-time PCR (qPCR), we found that *Galnt3* is the major O-glycosyltransferase expressed in the secretory cells of salivary glands. Additionally, 16S rRNA gene sequencing revealed that the loss of *Galnt3* resulted in changes in the structure, composition and stability of the oral microbiome. Moreover, we identified the major secreted salivary mucin, Muc10, as an in vivo

substrate of Galnt3. Given that mucins and their O-glycans are known to interact with various microbes, our results suggest that loss of *Galnt3* decreases glycosylation of Muc10, which alters the composition and stability of the oral microbiome. Considering that oral findings have been documented in HFTC patients, our study suggests that investigating GALNT3-mediated changes in the oral microbiome may be warranted.

.

The importance of the human microbiome throughout the body is only now being fully appreciated. In health, the microbiome interacts synergistically with the host to contribute to normal tissue functions as well as to protect from pathogen colonization (1,2). Alterations in the composition of the microbiome have been shown to be involved in various disease states, including inflammatory diseases of the digestive tract (3,4) and diseases of the oral cavity. At this site, dysbiotic changes in the microbiome are associated with dysregulated immune responses which lead to the common oral disease periodontitis (2,5-7).

The secreted mucosal membrane is a key point of interaction with the microbiome. This protective layer, which is present along most internal epithelial surfaces of the body, forms a barrier that mediates interaction with the microbiota and confers physical protection (8,9). The main components of this barrier include mucins, proteins with unique rheological properties conferred by the abundant O-glycans present throughout their repetitive domains. O-glycans on mucins bind water to form hydrated gels that line and protect internal epithelial surfaces (8,9). Additionally, mucins and their associated O-glycans bind microorganisms to modulate clearance, attachment and the ability to form biofilms (10-12). The importance of mucins and O-glycans in digestive system health is illustrated by studies in model organisms demonstrating that loss of the major intestinal mucin Muc2 or disruption of O-glycan biosynthesis results in spontaneous colitis, colon cancer and susceptibility to inflammatory conditions of the digestive tract (13-18). However, little is known regarding how individual mucins influence the establishment and composition of the microbiome.

Mucins and O-glycans have been conserved throughout evolution, suggesting important roles in many diverse biological processes (19-22). O-glycosylation is controlled by a family of enzymes known as the UDP-GalNAc:polypeptide N-acetylgalactosaminyltransferases (Galnts) that catalyze the addition of GalNAc to the hydroxyl group of serine or threonine, the first committed step in O-glycan biosynthesis (23,24). Members of this large family display differential tissue- and cell-specific expression patterns and unique substrate preferences, suggesting that each family member may be responsible for the proper glycosylation of specific proteins in vivo (23,25,26). Studies in model organisms have shown that certain Galnts are required for viability and involved in conserved biological processes, such as cell adhesion, secretion and cell signaling events (21,27-34). In humans, mutations in one family member, *GALNT3*, are responsible for the disease hyperphosphatemic familial tumoral calcinosis (HFTC), characterized by hyperphosphatemia, altered bone density and the development of subdermal calcified tumors (35). GALNT3-mediated glycosylation of the phosphate-regulating hormone FGF23 within osteocytes of the bone is presumed to protect FGF23 from protease cleavage under normal conditions; loss of the GALNT3

glycosyltransferase results in inactivating cleavage of FGF23 and dysregulation of phosphate homeostasis. A mouse model of this disease that is deficient for *Galnt3* recapitulates many disease phenotypes, including Fgf23 inactivating cleavage and hyperphosphatemia (36). While both males and females displayed these HFTC hallmark phenotypes, only males displayed growth retardation, infertility and increased bone density (36,37). The reasons for these gender-specific differences are currently unknown.

Interestingly, *GALNT3* (*Galnt3* in mice) is abundantly expressed in other tissues and thus may have a role in other parts of the body that could contribute to disease pathology (21,23). Here, we identify *Galnt3* as the major family member expressed in adult mouse salivary glands, which are responsible for producing the components of saliva, including mucins. Interestingly, we show that loss of *Galnt3* results in dramatic changes in the composition and structure of the oral microbiome. We further identify the major secreted mucin Muc10 as an in vivo and in vitro substrate of Galnt3. Our results demonstrate for the first time that the loss of a single glycosyltransferase can alter the oral microbiome, possibly through altered glycosylation of a major salivary mucin. Given the importance of the microbiome to health and disease, our study suggests that investigation of the oral microbiome in patients with mutations in *GALNT3* may be warranted to have a more comprehensive understanding of disease pathology.

Results

Galnt3 is the most abundant *Galnt* in the adult submandibular gland

Previous studies have shown that *Galnt3* is abundantly expressed in other tissues throughout the body, including the salivary glands (23,38). To begin to interrogate the relative abundance and temporal expression of *Galnt3* in the submandibular glands (SMGs), we investigated expression levels of each *Galnt* family member at three embryonic stages (E13, E15, E17), two early postnatal stages (P2, 1 wk), and three adult stages (4 wks, 8 wks, 12 wks) by performing qPCR (Fig. 1 and Fig. S1). At embryonic day 13 (E13), *Galnt1* is the most abundantly expressed isoform, followed by *Galnt2* and *Galnt11* (Fig. 1A). At E15 and E17, *Galnt2* becomes the most abundantly expressed isoform, followed by *Galnt1* at E15 and *Galnt4* and *Galnt1* at E17 (Fig. 1A). Interestingly, a dramatic change in *Galnt* expression occurs after birth as *Galnt3* and *Galnt12* are the most abundantly expressed isoforms at postnatal day 2 (P2) and 1 wk of age (Fig. 1B and Fig. S1A). Moreover, *Galnt3* expression continues to increase into adulthood, where it is by far the most abundant isoform at 4 wks, 8 wks and 12 wks of age (Fig. 1B and Fig. S1A), in both males and females (Fig. S1B). In situ hybridization revealed that *Galnt3* expression is confined to the acinar cells (detected with Aqp5) of the SMGs, the cells responsible for producing the secreted components of the saliva (Fig. 1C).

Previous work has shown that one of the most abundantly expressed *Galnts* during embryonic stages (*Galnt1*) plays key roles during SMG growth and development (28). This led us to examine the possibility that *Galnt3*, the most abundant isoform in adult SMGs, may play a role in adult SMG function. To investigate this, we crossed heterozygous *Galnt3*-deficient ($Galnt3^{+/-}$) animals to generate homozygous *Galnt3*-deficient ($Galnt3^{-/-}$) animals and wildtype (*WT*) littermate controls. $Galnt3^{-/-}$ mice have been previously generated as a mouse model for HFTC and were found to have hyperphosphatemia, inappropriately normal levels of $1,25(OH)_2D$, and decreased levels of circulating

intact Fgf23, similar to what is seen in HFTC patients (36). As it is well-documented that rodent SMGs become morphologically distinct between males and females beginning at approximately 6 weeks of age (with males developing many more granular convoluted tubules than females) (39), all future experiments analyzed male and female animals separately. Upon examination of SMGs at 8 wks of age, we found no significant differences in gland weight (Fig. S2A and B) or SMG morphology (Fig. S2C) between *WT* and *Galnt3*$^{-/-}$ mice for either sex. Previous studies from our lab investigating the role of another member of this family in the SMG found an induction of ER stress upon loss of *Galnt1* (28). To determine if the loss of *Galnt3* also induced ER stress and the unfolded protein response (similar to that seen in *Galnt1*$^{-/-}$ SMGs; (28)), we next examined Xbp1 mRNA splicing. Quantification of the ratio of spliced Xbp1 (Xbp1s) to unspliced Xbp1 (Xbp1u) revealed no statistically significant differences between *WT* and *Galnt3*$^{-/-}$ SMGs for either sex (Fig. S2D-G), indicating that the loss of *Galnt3* does not result in ER stress. Additionally, we performed a number of analyses of adult SMG function. *Ex vivo* analysis of SMG salivary flow rate, volume of saliva secreted, and ion content of saliva revealed no significant differences between *WT* and *Galnt3*$^{-/-}$ animals for either sex (Fig. S3A-F). These results indicate that the loss of *Galnt3* does not result in overt differences in SMG size, morphology or function via these assays.

Loss of *Galnt3* alters the oral microbiome

In addition to its role in hydration and lubrication of the oral cavity, saliva is believed to play a role in regulating the oral microbiota (40). This led us to investigate the effect of loss of *Galnt3* on the microbial communities within the oral cavity through the characterization of the local microbiome. Microbiome studies analyze the numbers and types of distinct microbial taxa as well as their relative abundances in order to provide assessments of microbial community structures. We collected oral mucosal samples as previously described (41) from individual *WT* and *Galnt3*$^{-/-}$ mice at both 8 wks and 12 wks of age and performed 16S rRNA gene sequencing. Beta diversity comparisons of the microbial community structure within the oral cavity across genotypes and age groups were assessed using the Theta Yue and Clayton (θ YC) distance (which takes into account the specific bacterial species present as well as their relative abundances within the communities being compared) and visualized on 2D principal coordinates analysis (PCoA) plots (Fig. 2). We also analyzed alpha diversity within each genotype and age group (which measures the number of bacterial taxa and their relative proportions within a particular group), using the non-parametric version of the Shannon index (Fig. S4).

Through beta diversity analysis, we found distinct microbial communities in *Galnt3*$^{-/-}$ male samples compared to *WT* at both 8 wks and 12 wks of age (Fig. 2A and B). PCoA plots demonstrate that there was significant clustering and separation of male *Galnt3*$^{-/-}$ microbial communities from male *WT* communities ($p < 0.05$ as determined by AMOVA; Fig. 2A and B). In contrast to male samples, no significant differences between the community structure of *WT* and *Galnt3*$^{-/-}$ female samples were observed for either age (Fig. 2C and D, Fig. S5A and B). No significant differences in alpha diversity were observed for either males or females (Fig. S4A-D). These results indicate that there are significant microbial shifts in the oral

microbiome community structure in males upon loss of *Galnt3*.

Examining the composition of the oral microbiome in more detail, we found specific changes in the relative abundance of select taxa between male *WT* and *Galnt3*$^{-/-}$ animals. At 8 wks of age, two operational taxonomic units (OTUs) from the *Pasteurellaceae* family (which had a high percentage of similarity with the species *Muribacter muris* and *Rodentibacter heidelbergensis*), were over-represented in *WT* samples, while a *Lactobacillus sp. (L. faecis)* and two other low abundance OTUs (an unclassified *Lachnospiraceae* sp. and a *Candidatus Saccharibacteria/TM7* sp.) were increased in *Galnt3*$^{-/-}$ samples (Fig. 2E). At 12 wks of age, a *Streptococcus sp. (S. danieliae)* was over-represented in *WT* samples, while a *Pasteurellaceae sp.* (*Rodentibacter heidelbergensis*) became over-represented in *Galnt3*$^{-/-}$ samples (Fig. 2F). Interestingly, 12 wk *Galnt3*$^{-/-}$ samples continued to show an increase in *Lactobacillus sp. (L. faecis)* as compared to *WT* (Fig. 2F). It is notable that these data come from mice of both genotypes housed across multiple cages, eliminating the possibility that the distinct microbial communities are due to cage-specific effects. We next examined the stability of the oral microbiome in individual adults of each genotype over time. Similar to previous studies in mice and humans (6,42), the microbial community structure of *WT* animals was stable over time, as no significant differences were found between 8 wk and 12 wk samples for either male or female animals (Fig. 3A and B, Fig. S5C and D). Likewise, no significant differences were seen in alpha diversity (Fig. S4E and F). However, significant differences in community structure were seen over time in *Galnt3*$^{-/-}$ animals (Fig. 3C and D). For both males and females, 8 wk *Galnt3*$^{-/-}$ oral mucosal communities significantly separated from 12 wk *Galnt3*$^{-/-}$ communities, and these differences were found to be statistically significant by AMOVA ($p < 0.05$) (Fig. 3C and D). Investigating age-related differences in relative abundance of bacterial taxa in more detail in male *Galnt3*$^{-/-}$ samples, we found that the OTUs *Pasteurellaceae sp. (Muribacter muris)* and *Pasteurellaceae sp. (Rodentibacter heidelbergensis)* were over-represented in 12 wk samples as compared to 8 wk (Fig. 3E). Similarly, these two OTUs belonging to the *Pasteurellaceae* family were also more abundant in 12 wk female *Galnt3*$^{-/-}$ samples as compared to 8 wk, while a *Streptococcus sp. (S. danieliae)* was over-represented at 8 wks (Fig. 3F). While there were no significant changes in alpha diversity in *Galnt3*$^{-/-}$ males over time, there was a significant increase in alpha diversity in 12 wk *Galnt3*$^{-/-}$ females (Fig. S4G and H). These results indicate that the composition of the oral microbiome is less stable over time upon loss of *Galnt3* in both males and females.

We also compared the microbiomes between *WT* males and females at each time point. While a difference in structure was seen at 8 weeks of age (Fig. S6A), this difference was no longer significant by 12 weeks of age (Fig. S6B). Examination of the taxonomy data reveals that the differences at 8 weeks of age are driven by differences in the relative abundance of the major taxa, rather than the presence or absence of unique taxa (Fig. S6C and D). Likewise, there were no significant differences in alpha diversity between *WT* males and females at either age (Fig. S4I and J).

Galnt3 glycosylates Muc10

To investigate how the loss of *Galnt3* (which encodes an O-glycosyltransferase that catalyzes the

first committed step in O-glycan biosynthesis) may be influencing the composition and stability of the microbiome, we next examined the O-glycans that are normally present within the SMG using lectins that are specific to O-glycan structures. Previous studies have documented distinct gender differences in the expression of the *ST3Gal1* gene (which encodes a sialyl transferase that adds sialic acid in an α2,3 linkage to glycans), with this gene being 22 fold more abundantly expressed in the SMGs of females vs. males (*(https://sgmap.nidcr.nih.gov/cgi-bin/sgexp11.plx?ind=1&gn=St3gal1*). Indeed, female SMGs stained abundantly with the lectin *Maackia amurensis* agglutinin (MAA) (Fig. 4A), which detects α2,3 linked sialic acid linked to either N- or O-glycans (43). This staining was seen in the acinar cells of the SMG (labeled with the marker Acinar-1) and was specifically removed upon treatment with an enzyme that removes sialic acid (neuramindase; NM), indicating specificity (Fig. 4A). Staining with MAA was also seen in male SMG acinar cells, but to a lesser extent (Fig. 4B). We next used the lectin peanut agglutinin (PNA) (which detects the non-sialylated core 1 structure Galβ1,3GalNAc of O-glycans) in the presence or absence of NM treatment to determine the degree to which O-glycans are sialylated in both *WT* females and males (Fig. 4C and D). As shown in Fig. 4D, PNA staining is abundantly present within the acinar cells (labeled with the Acinar-1 marker) of males SMGs with or without NM treatment, indicating the presence of non-sialylated core 1 O-glycans in males. However, PNA staining was only detected in female SMGs after NM treatment, indicating that all core 1 O-glycans are modified with sialic acid in females (Fig. 4C). PNA staining in both males and females could be competed away by incubation with galactose, indicating specificity (Fig. S7). Similar results were obtained on western blots of SMG extracts, where female samples showed no PNA reactivity in the absence of NM treatment, whereas male samples had PNA reactivity with or without NM treatment (Fig. 4E and F). Taken together, these results indicate that distinct differences exist between males and females in the structure of the O-glycans present within the SMGs, with males having both sialylated and non sialylated core 1 O-glycans and females having core 1 O-glycans that are predominantly sialylated. Therefore, all further analysis of PNA-reactive O-glycans in females was performed on samples that had been treated with NM, whereas male samples were not treated with NM.

We next set out to compare changes in glycans present in *WT* and *Galnt3*$^{-/-}$ SMGs via confocal microscopy. As shown in Fig. 5A and B, loss of *Galnt3* did not result in obvious changes in MAA staining in either males or females. However, a dramatic decrease in PNA-reactive O-glycans specifically in the acinar cells of male SMGs was seen upon loss of *Galnt3* (Fig. 5C). In contrast to males, female *Galnt3*$^{-/-}$ SMGs (treated with NM) did not show a noticeable change in PNA-reactive O-glycan staining within the acinar cells relative to *WT* via confocal imaging (Fig. 5D). These results suggest that the loss of *Galnt3* results in a major change in PNA-reactive O-glycans normally present within the acinar cells of male SMGs.

We next set out to identify the potential protein targets of Galnt3 in the SMGs. Mucins are heavily O-glycosylated proteins known to be the major protein products produced by the salivary glands and are thought to mediate interactions with the microbiome (12,44). Previous studies have identified Mucin 10 (Muc10; also known as mouse submandibular gland mucin and Proline rich, lacrimal 1) as the major mouse SMG mucin and

have shown that it localizes to the acinar cells of adult SMGs (45,46). Here, we examined in detail the postnatal gene expression of *Muc10* using qPCR (Fig. 6A). At all five stages examined (P2, 1 wk, 4 wks, 8 wks, and 12 wks), *Muc10* was found to be abundantly expressed, with its expression increasing in adult stages (Fig. 6A). qPCR to other mucins revealed that *Muc10* was by far the most abundantly expressed mucin within the SMGs (Fig. 6A-D). Additionally, we confirmed that Muc10 is also expressed in acinar cells (detected with Acinar-1) of SMGs (Fig. 6E) similar to *Galnt3*, suggesting that Muc10 may be a direct target of Galnt3.

Given the abundant expression of *Muc10* within acinar cells of the SMGs, we next set out to determine if O-glycosylation of Muc10 was specifically affected by the loss of *Galnt3*. We performed western blots of 8 wk *WT* and *Galnt3*$^{-/-}$ SMG extracts probing for PNA and Muc10 (Fig. 7). In *WT* male SMGs, two major PNA bands were detected (Fig. 7A). However, in *Galnt3*$^{-/-}$ SMGs, the lower molecular weight PNA-reactive band was greatly reduced or absent, suggesting that this protein is specifically glycosylated by Galnt3. Interestingly, probing the same western blot for Muc10 revealed that the Muc10 band overlaps with the lower PNA-reactive band in *WT* SMGs, suggesting that Muc10 may be this highly O-glycosylated band (Fig. 7A). In support of this, immunoprecipitation of Muc10 from *WT* SMGs revealed that it does contain PNA-reactive O-glycans (Fig. S8). Additionally, the Muc10 band in *Galnt3*$^{-/-}$ SMGs no longer overlaps with PNA staining and runs at a reduced size, further suggesting the loss of O-glycans on this protein (as these sugar modifications can account for a significant change in molecular weight). These results strongly suggest that Muc10 is specifically O-glycosylated by Galnt3 in male SMGs. Western blots of 8 wk female SMGs did not reveal the same PNA banding pattern seen in *WT* males and did not result in the loss of specific PNA-reactive bands as seen in male *Galnt3*$^{-/-}$ SMGs (Fig. 7B). However, the loss of *Galnt3* in female SMGs did result in PNA reactivity with altered mobility (Fig. 7B). Additionally, Muc10-reactive bands ran as large smears that overlapped in position with PNA staining in *Galnt3*$^{-/-}$ female SMGs (Fig. 7B). These results suggest that Muc10 is also a substrate for Galnt3 in female SMGs and that while the loss of *Galnt3* does not result in a complete disruption of O-glycosylation (as detected by PNA), it may alter the patterns of O-glycosylation in more subtle ways in females.

To further investigate the ability of Galnt3 to glycosylate Muc10, we performed in vitro enzymatic assays using recombinant murine Galnt3 and acceptor peptides from Muc10. Standard transferase assays revealed that Galnt3 was able to glycosylate four different peptides derived from Muc10 (Fig. 7C and D), providing further evidence that Muc10 is a substrate for Galnt3 in the SMGs. Interestingly, Galnt3 had specific site preferences among the Muc10 peptides, showing highest activity toward the Muc10-s and Muc10-264 peptides, followed by Muc10-273 and Muc10-l (all of which are derived from the repetitive domain of Muc10). Galnt3 did not show activity toward the Muc10-10 peptide (Fig. 7C and D, Fig. S9 and Fig. S10). These results are in agreement with predicted site preferences previously determined for Galnt3 (47). Taken together, our results demonstrate that loss of *Galnt3* leads to changes in the composition of the oral microbiome in males, possibly due to changes in the glycosylation status of the major salivary mucin Muc10. Moreover, loss of *Galnt3* results in altered stability of the oral microbiome in both males and females. Given that mutations in

GALNT3 cause the human disease HFTC and that *Galnt3*$^{-/-}$ mice serve as a model for this disease, our results suggest that HFTC patients may also have alterations in their oral microbiome that could contribute to documented disease pathology in the oral cavity (Suppl. Table I).

Discussion

Here we demonstrate that the gene responsible for HFTC alters the composition and stability of the oral microbiome. *Galnt3* is the most abundantly expressed member of the *Galnt* family in the acinar cells of adult SMGs, which produce the components of the saliva that lines and protects the oral cavity. Loss of *Galnt3* resulted in dramatic changes in the predominant bacterial taxa present, as well as significant changes in the overall composition of the oral microbiome in males. Moreover, we found that while the composition of the oral microbiome was stable over time in *WT*, this stability was lost in both male and female *Galnt3*-deficient animals, suggesting that the presence of Galnt3-initiated glycans confers stability to the endogenous microbial communities. Previous studies have documented the notable stability of the oral microbiome in association with health (42), as well as how dysbiotic changes in the oral microbiome can trigger an increase in inflammation leading to periodontitis (2,5-7). Indeed, bacterial homoeostasis is a crucial part of oral health, as several prevalent oral diseases such as dental caries, periodontitis and oral candidiasis are associated with local microbial dysbiosis (48,49). Additionally, changes in the oral microbiome in certain genetic disorders underlie local inflammation and pathology observed within the oral cavity (50,51). As some clinical reports of HFTC patients have included oral findings (Suppl. Table S1), our results in the mouse model of this disease may provide insight into how the systemic loss of *GALNT3* may result in pathology within the oral cavity.

We further demonstrate that changes in the composition of the oral microbiome upon loss of *Galnt3* are associated with changes in the glycosylation status of the major salivary mucin, Muc10. While there were no overt phenotypic or functional differences between *WT* and *Galnt3*$^{-/-}$ SMGs, there was a significant loss of O-glycans within the acinar cells of male *Galnt3*$^{-/-}$ glands. This change in glycosylation was in part due to dramatic changes in the glycosylation status of Muc10 in males. Moreover, we show that Galnt3 glycosylates specific regions of Muc10 in vitro, in accordance with predicted site preferences based on bioinformatic analyses, establishing Muc10 as an in vivo and in vitro substrate of Galnt3. Interestingly, we did not see significant changes in the abundance of O-glycans in female *Galnt3*$^{-/-}$ SMGs, just as we did not see significant changes in the composition of the oral microbiome in females. However, the females did display changes in Muc10 mobility, suggesting more subtle changes in its glycosylation pattern. It is worth noting that the core 1 O-glycans present in *WT* SMGs differ between males and females, with female O-glycans being predominantly capped with sialic acid. How gender-specific differences in the degree of sialylation of proteins may influence various biological processes remains to be investigated.

Our study supports a model where altered glycosylation of a major salivary mucin may lead to alteration and instability of the oral microbiome, which has physiological implications regarding host-microbial interactions at this interface. This model is further supported by many studies documenting the interaction of bacteria with mucins and O-glycans, influencing their clearance

and ability to colonize (10,11). Additionally, glycans on mucins can interact with bacterial receptors to influence microbial behavior and signaling (52,53). Interestingly, the human ortholog of Muc10 (MUC7/MG2) has documented roles in bacterial binding and aggregation (54-56), suggesting that this mucin may play a role in maintaining the stability of the oral microbiome in health. Indeed, a recent study demonstrated that a human oral microbe recognizes α 2,3 sialylated core 1 structures on the human ortholog of Muc10 (MUC7) (57), highlighting the importance of sialylated O-glycans in bacterial recognition. Given the dramatic differences in the degree of sialylation of O-glycans seen between males and females, it will be interesting to investigate gender-specific glycosylation patterns and how they may influence biological phenotypes.

In summary, we have found changes in the composition and stability of the oral microbiome in the mouse model of the human disease HFTC. Whether HFTC patients (who lack functional GALNT3) also have changes in the composition of their oral microbiome is currently unknown. However, *GALNT3* is abundantly expressed in human SMGs (21) and a number of clinical studies have noted oral findings in HFTC patients, including caries, gingivitis, periodontitis and changes in enamel (Suppl. Table S1). Given our results and the obvious importance of the microbiome in health and organ function, our study suggests that examining the oral microbiome and oral phenotypes in HFTC patients may be informative.

Experimental procedures

Animal breeding and genotyping

The *Galnt3*-deficient mice were a kind gift from Dr. Michael J. Econs (36). *Galnt3*-deficient mice were backcrossed into the C57BL/6MHsd inbred mouse background for at least six generations before analysis. Heterozygous *Galnt3* animals (*Galnt3*$^{+/-}$) were crossed to generate wildtype (*WT*) and homozygous *Galnt3*-deficient (*Galnt3*$^{-/-}$) siblings to be used for all experiments. Genomic DNA was extracted from mouse ear punches using the DNeasy Blood & Tissue Kit (Qiagen #69506) and PCR was performed as previously described (36). Experimental procedures were reviewed and approved by the Animal Care and Use Committee of the National Institutes of Health (ASP #17-833).

Semi-quantitative Real-Time PCR

RNA was isolated and purified using the PureLink™ RNA Mini Kit (Invitrogen #12183018A). cDNA was synthesized using iScript™ Reverse Transcription Supermix (Bio-Rad). Primers for *Galnt* and *Mucin* genes were designed using Beacon Designer software and are shown in Supplementary Tables S2 and S3, respectively. qPCR was performed for 40 cycles (95°C for 10 seconds and 62°C for 30 seconds) using SYBR-green PCR Master Mix, either 1 ng (*Galnt* genes) or 10 ng (*Mucin* genes) of each cDNA sample, and the CFX96 Real-Time system (Bio-Rad). Gene expression was normalized to *29S* rRNA. Reactions were run in triplicate and repeated using three or more animals.

Histology

8 wk mouse submandibular glands were fixed in 4% PFA/PBS overnight at 4°C, transferred to 70% ethanol and stored at 4°C. Paraffin-embedded tissue sections (5 μm) were used for hematoxylin/eosin (H&E) staining, in situ hybridization, and immunofluorescent staining.

In situ hybridization

Primers of *Galnt3* probes were designed using Beacon Designer software. Probes were amplified by KOD kit (TAKARA) and purified by QIAquick spin kit (Qiagen). Digoxigenin-11-UTP-labeled single-stranded RNA probes were prepared using DIG RNA labeling kit (Sigma-Aldrich #11175025910). Fixed, paraffin-embedded SMG sections (5 μm) were dewaxed at 60°C for 10 minutes followed by 3 changes of xylene substitute (Sigma #A5597). Sections were rehydrated with 2 changes of 100% ethanol and single changes of 90%, 70% and 50% ethanol. Sections were fixed by 4% PFA/PBS for 5 minutes, followed by 10 mg/ml Proteinase K (Sigma #4850) treatment for 30 minutes at 37°C. After post-fixing with 4% PFA/PBS for 5 minutes, sections were dehydrated in ethanol series (50%, 70%, 90% and 100%). Hybridization was performed by incubating sections with 50 ng *Galnt3* RNA DIG labeled anti-sense or sense probes in 25 μl hybridization buffer for 10 minutes at 85°C, then overnight at 50°C. After washing the next day, sections were treated with 10 mg/ml RNase A in 10 mM Tris-HCl (pH7.5)/500 mM NaCl for 15 minutes at 37 °C. Following washing, sections were blocked with 1% Blocking reagent (Roche, #1096176) for 30 minutes at room temperature, then incubated with anti-DIG-POD antibody (Roche; 1:100) and Aquaporin-5 primary antibody (Calbiochem, #178615; 1:100) overnight at 4°C. On day 3, sections were washed, then incubated with Alexa Fluor 647®-conjugated anti-rabbit IgG (Jackson ImmunoResearch; 1:400) for 1 hour at room temperature. Following washing, sections were incubated with Tyramide Signal Amplification plus Cy3 (TSA, PerkinElmer; 1:50 in amplification buffer) for 30 minutes at room temperature. After washing, sections were nuclear counterstained with Hoechst 33342 (Invitrogen #H3570; 1:10000) and mounted in aqueous Fluro-Gel medium (Electron Microscopy Sciences #17985-10). Sections were visualized on a Nikon A1R confocal microscope and images were processed in NIH Fiji.

Immunofluorescent staining

Fixed, paraffin-embedded tissue sections (5 μm) were deparaffinized by incubating slides at 60°C for 10 minutes, followed by 3 washes in xylene substitute (Sigma #A5597). Sections were rehydrated with single changes of 100%, 90%, 70%, 50%, and 30% ethanol and deionized water. Antigen retrieval was performed by incubating slides in 5% urea and 50 mM β-mercaptoethanol for 10 minutes at 95°C, followed by 40 minutes of cooling. For female samples to be probed with PNA (except where noted), sections were treated with 20 mU neuraminidase (New England BioLabs #P0720) overnight at 37°C. Sections were blocked with 10% donkey serum, 1% BSA, and M.O.M blocking reagent (Vector Laboratories #FMK-2201). Where noted in the text and figures, some male samples were also treated with neuraminidase via the same procedure. Primary antibodies were diluted in PBS-0.1% Tween-20 plus M.O.M. protein reagent and incubated overnight at 4°C for male samples or for 2 hours at room temperature for female samples. Primary antibodies used were Muc10 (Everest Biotech #EB10617; 1:200) and Acinar-1 (Developmental Studies Hybridoma Bank #3.7A12; 1:20). After washing, sections were incubated for 1.5 hours at room temperature with either TRITC-conjugated *Maackia amurensis* lectin (MAA) (EY Laboratories #R-7801-2; 1:100) or FITC-conjugated peanut agglutinin (PNA) (Vector Laboratories #FL-1071; 1:200), Cy™3-conjugated anti-goat IgG (Jackson ImmunoResearch; 1:400), and Alexa Fluor 647®-

conjugated anti-rat IgG (Jackson ImmunoResearch; 1:400). For sugar inhibition of PNA, 0.2 M galactose (Sigma-Aldrich #G0750) was incubated with FITC-labeled PNA for 1 hour at room temperature before applying to slides. Nuclear counterstaining was done using Hoechst 33342 (Invitrogen #H3570; 1:10000) for 3 minutes at room temperature. Stained sections were mounted in aqueous Fluro-Gel medium (Electron Microscopy Sciences #17985-10) and visualized on a Nikon A1R confocal microscope. Images were processed in Fiji and representative stacked section confocal images are shown in each figure. FITC-labeled PNA was pseudo-colored to red and TRITC-labeled MAA was pseudo-colored to green in NIH Fiji (Fig. 4 A&B, Fig. 5, Fig. S6).

Immunoprecipitation

Immunoprecipitation was performed using TrueBlot® Anti-Goat IgG Magnetic Beads (Rockland Immunochemicals Inc. #00-1844) according to the manufacturer's instructions with modifications. 8 wk *WT* SMG lysates were prepared in RIPA buffer with sonication. 25 µg SMG lysates were combined with 5 µg Muc10 antibody (Everest Biotech #EB10617), diluted to 250 µl in RIPA buffer, and incubated overnight at 4°C with mixing. The next day, beads were washed with RIPA buffer. 200 µl (1 mg) pre-washed beads were then combined with the pre-formed SMG lysate/antibody complexes and incubated overnight at 4°C with mixing. Next, beads were collected and the supernatant was removed, followed by washing with RIPA buffer. Beads were then resuspended in RIPA buffer and SDS loading dye (containing 1/25 dilution of β-mercaptoethanol) and heated at 95°C for 10 minutes, followed by cooling on ice for 10 minutes. The supernatant (containing the target antigen) was then removed from the beads and used for SDS-PAGE and Western blotting as described in the next section.

Western blotting

PNA (Arachis hypogaea lectin, EY Laboratories #L-2301) was labeled with IRDye 680LT (LI-COR #928-38066). 8 wk SMGs from littermate *WT* and *Galnt3*$^{-/-}$ animals were lysed in RIPA buffer with sonication. SMGs from male and female animals were treated with 6.25 mU neuraminidase where noted in the text and figures (New England BioLabs #P0720) for 1 hour at 37°C. Samples were analyzed by SDS-PAGE under denaturing and reducing conditions and transferred to nitrocellulose membranes. Membranes were blocked with 1:1 PBS/Odyssey Blocking Buffer (LI-COR #927-4000) and probed with Muc10 (Everest Biotech #EB10617; 1:2000). After washing, membranes were probed with IRDye 680LT-conjugated PNA (1:10000) and IRDye 800CW-conjugated anti-goat IgG (LI-COR #925-32214; 1:5000). Membranes were scanned using a LI-COR Odyssey Infrared Imaging System.

Xbp1 mRNA splicing PCR

PCR primers used to detect splicing of Xbp1 were previously published (28). PCR was performed for 35 cycles (94°C for 30 seconds, 61°C for 30 seconds, 72°C for 90 seconds) using 10 ng of each cDNA sample and a Veriti™ thermal cycler (Applied Biosystems). PCR products were identified using 4-20% TBE gels and ethidium bromide. Negative images of gels are shown. NIH Fiji was used to measure band intensity and normalized ratios of spliced Xbp1/unspliced Xbp1 were determined (ratio for *WT* controls set to 1).

Enzyme Assays

Expression of recombinant murine Galnt3 was performed as described previously (38) using COS7 cells. Assays for Galnt3 activity were performed as described previously (38) using 5 µl media from COS7 cells transfected with murine Galnt3. Muc10 and EA2 peptide substrates were synthesized by Peptide 2.0 (Fig. 5D, S6). Reactions were run for 1.5 hours at 37°C, then quenched with 30 mM EDTA. Glycosylated products were separated from unincorporated UDP-^{14}C-GalNAc by anion exchange chromatography using AG1-X8 resin columns (Bio-Rad #1401454), and product incorporation was determined by liquid scintillation counting. Background values were obtained from reactions using media from COS7 cells transfected with empty vector and subtracted from each experimental value. Assays for each peptide substrate were run in triplicate and repeated three times.

Ex vivo perfused SMG

Ex vivo SMG saliva secretions were collected by modifying the ex vivo mouse SMG perfusion technique (58). In brief, mice were anesthetized by chloral hydrate injection (400 mg/kg i.p.) and all branches of the common carotid artery were ligated, except for the artery supplying blood to SMG. Intact glands were then removed and transferred to a temperature-controlled perfusion chamber at 37°C. Then, the common artery was cannulated with a 31G cannula and perfused with a solution containing the muscarinic receptor agonist (CCh, 0.3 µM) plus β-adrenergic agonist (IPR, 1.0 µM). The SMG duct was placed in a calibrated glass capillary tube. Perfusion rate was kept at 1.0 ml/min with a peristaltic pump (IPC-8, ISMATEC, Wertheim, Germany). The ex vivo perfusion solution contained (in mM): 4.3 KCl, 120 NaCl, 25 $NaHCO_3$, 1 $CaCl_2$, 1 $MgCl_2$, 5 glucose and 10 Hepes, pH 7.2 (gassed with 95% O_2/5% CO_2). Secreted saliva samples were collected and stored at –80°C until analyzed.

Ion concentrations in SMG secretions

Sodium and potassium concentrations were analyzed by atomic absorption spectroscopy (3030 spectrophotometer, PerkinElmer, Waltham, MA). Chloride activity was measured using a chloride electrode (9617BNWP, Thermo Fisher Scientific) with 4-Star Plus pH/ISE Benchtop Multiparameter Meter (Thermo Fisher Scientific, Waltham, MA).

Sample collection and DNA extraction for microbiome analysis

To allow a comprehensive sampling of oral mucosal surfaces, we collected oral mucosal samples from 8 wk and 12 wk mice. We utilized ultra-fine polystyrene swabs to obtain microbial samples from the murine oral cavity for 30 s, then these samples were placed in 150 µl of TE buffer and stored at -80 °C until processing. DNA was extracted following a modified protocol of the DNeasy Blood and Tissue Kit (Qiagen) as previously described (41).

16S rRNA gene-based sequencing and bioinformatic analyses

Library generation was performed using Eppendorf liquid handling robots. The V4 region of the 16S rDNA gene (515F-806R) was sequenced for oral mucosal samples; generating paired-end, overlapping reads on the Illumina MiSeq platform (59). Sequencing data was processed using the software Mothur (60). Briefly, reads were quality filtered, assembled into contigs and only reads from 200-400 bp in length were kept. Then, our processing continued following the MiSeq SOP

pipeline (https://www.mothur.org/wiki/MiSeq_SOP) as described (61). Operational taxonomic units (OTUs) were defined at a 97% similarity and genus-level taxonomical classification was achieved. However, we further informed our classification down to species-level through blasting the reference sequence of each OTU against the NCBI 16S rRNA database using BLAST, as previously described (41). Beta diversity was assessed using the Theta Yue and Clayton (θ YC) distance. Alpha diversity was evaluated using the non-parametric version of the Shannon diversity index. Both diversity measurements were calculated as implemented in mothur. All sequence data from this study have been submitted to NCBI SRA database under SRA accession number PRJNA547610.

Statistical analysis

Error bars represent standard deviation for values obtained from three or more mice. Student's t-test and Mann-Whitney test were used to calculate p values. For microbiome analyses, AMOVA (analysis of molecular variance) was used to test for differences in community structure. LEfSe (62) was used to test for differences in relative abundance of taxa, considering 0.05 as the α value for statistical testing.

Acknowledgements. We would like to thank our colleagues for many helpful discussions. We would like to thank the NCI Microbiome and Genetics Sequencing Core for 16S sequencing and processing. This work was supported by the Intramural Research Program of the NIDCR, National Institutes of Health (Z01-DE000713 to K.G.T.H. and ZIA-DE000738 James E. Melvin). This research was also supported in part by the NIDCR Veterinary Resources Core (ZIC DE000740-05), the NIDCR Imaging Core (DE000750-01) and the Chilean National Fund for Scientific and Technologic Development (FONDECYT) (Grant # 11180505 to L.A).

Conflict of interest: The authors declare no conflicts of interest.

Author Contributions: G.P., E.T. and K.G.T.H. designed and planned the research. G.P. performed all mouse experiments, with input from E. T. and K.G.T.H. L.A. performed oral microbiome analyses. T.M. and T.M. performed salivary flow and ion analyses. G.P., E.T. and K.G.T.H. analyzed and discussed the data. G. P. and K.G.T.H. wrote the paper with input from E. T. and L. A.

References

1. Kamada, N., Chen, G. Y., Inohara, N., and Nunez, G. (2013) Control of pathogens and pathobionts by the gut microbiota. *Nat Immunol* **14**, 685-690
2. Lamont, R. J., Koo, H., and Hajishengallis, G. (2018) The oral microbiota: dynamic communities and host interactions. *Nat Rev Microbiol* **16**, 745-759
3. Huttenhower, C., Kostic, A. D., and Xavier, R. J. (2014) Inflammatory bowel disease as a model for translating the microbiome. *Immunity* **40**, 843-854

4. Lamont, R. J., and Hajishengallis, G. (2015) Polymicrobial synergy and dysbiosis in inflammatory disease. *Trends Mol Med* **21**, 172-183
5. Abusleme, L., Dupuy, A. K., Dutzan, N., Silva, N., Burleson, J. A., Strausbaugh, L. D., Gamonal, J., and Diaz, P. I. (2013) The subgingival microbiome in health and periodontitis and its relationship with community biomass and inflammation. *ISME J* **7**, 1016-1025
6. Dutzan, N., Kajikawa, T., Abusleme, L., Greenwell-Wild, T., Zuazo, C. E., Ikeuchi, T., Brenchley, L., Abe, T., Hurabielle, C., Martin, D., Morell, R. J., Freeman, A. F., Lazarevic, V., Trinchieri, G., Diaz, P. I., Holland, S. M., Belkaid, Y., Hajishengallis, G., and Moutsopoulos, N. M. (2018) A dysbiotic microbiome triggers TH17 cells to mediate oral mucosal immunopathology in mice and humans. *Sci Transl Med* **10**
7. Griffen, A. L., Beall, C. J., Campbell, J. H., Firestone, N. D., Kumar, P. S., Yang, Z. K., Podar, M., and Leys, E. J. (2012) Distinct and complex bacterial profiles in human periodontitis and health revealed by 16S pyrosequencing. *ISME J* **6**, 1176-1185
8. Johansson, M. E., and Hansson, G. C. (2016) Immunological aspects of intestinal mucus and mucins. *Nature reviews. Immunology* **16**, 639-649
9. Johansson, M. E., Sjovall, H., and Hansson, G. C. (2013) The gastrointestinal mucus system in health and disease. *Nature reviews. Gastroenterology & hepatology* **10**, 352-361
10. Culp, D. J., Robinson, B., Cash, M. N., Bhattacharyya, I., Stewart, C., and Cuadra-Saenz, G. (2015) Salivary mucin 19 glycoproteins: innate immune functions in Streptococcus mutans-induced caries in mice and evidence for expression in human saliva. *J Biol Chem* **290**, 2993-3008
11. Frenkel, E. S., and Ribbeck, K. (2015) Salivary mucins protect surfaces from colonization by cariogenic bacteria. *Appl Environ Microbiol* **81**, 332-338
12. Frenkel, E. S., and Ribbeck, K. (2017) Salivary mucins promote the coexistence of competing oral bacterial species. *ISME J* **11**, 1286-1290
13. An, G., Wei, B., Xia, B., McDaniel, J. M., Ju, T., Cummings, R. D., Braun, J., and Xia, L. (2007) Increased susceptibility to colitis and colorectal tumors in mice lacking core 3-derived O-glycans. *J Exp Med* **204**, 1417-1429
14. Bergstrom, K., Liu, X. W., Zhao, Y. M., Gao, N., Wu, Q., Song, K., Cui, Y., Li, Y., McDaniel, J. M., Mcgee, S., Chen, W. C., Huycke, M. M., Houchen, C. W., Zenewicz, L. A., West, C. M., Chen, H., Braun, J., Fu, J. X., and Xia, L. J. (2016) Defective Intestinal Mucin-Type O-Glycosylation Causes Spontaneous Colitis-Associated Cancer in Mice. *Gastroenterology* **151**, 152-+
15. Fu, J., Wei, B., Wen, T., Johansson, M. E., Liu, X., Bradford, E., Thomsson, K. A., McGee, S., Mansour, L., Tong, M., McDaniel, J. M., Sferra, T. J., Turner, J. R., Chen, H., Hansson, G. C., Braun, J., and Xia, L. (2011) Loss of intestinal core 1-derived O-glycans causes spontaneous colitis in mice. *J Clin Invest* **121**, 1657-1666

16. Gao, N., Bergstrom, K., Fu, J., Xie, B., Chen, W., and Xia, L. (2016) Loss of intestinal O-glycans promotes spontaneous duodenal tumors. *Am J Physiol Gastrointest Liver Physiol* **311**, G74-83
17. Velcich, A., Yang, W., Heyer, J., Fragale, A., Nicholas, C., Viani, S., Kucherlapati, R., Lipkin, M., Yang, K., and Augenlicht, L. (2002) Colorectal cancer in mice genetically deficient in the mucin Muc2. *Science* **295**, 1726-1729
18. Wenzel, U. A., Magnusson, M. K., Rydstrom, A., Jonstrand, C., Hengst, J., Johansson, M. E., Velcich, A., Ohman, L., Strid, H., Sjovall, H., Hansson, G. C., and Wick, M. J. (2014) Spontaneous colitis in Muc2-deficient mice reflects clinical and cellular features of active ulcerative colitis. *PLoS One* **9**, e100217
19. Aoki, K., Porterfield, M., Lee, S. S., Dong, B., Nguyen, K., McGlamry, K. H., and Tiemeyer, M. (2008) The diversity of O-linked glycans expressed during Drosophila melanogaster development reflects stage- and tissue-specific requirements for cell signaling. *J Biol Chem* **283**, 30385-30400
20. Lang, T., Hansson, G. C., and Samuelsson, T. (2007) Gel-forming mucins appeared early in metazoan evolution. *Proc Natl Acad Sci U S A* **104**, 16209-16214
21. Schwientek, T., Bennett, E. P., Flores, C., Thacker, J., Hollmann, M., Reis, C. A., Behrens, J., Mandel, U., Keck, B., Schafer, M. A., Haselmann, K., Zubarev, R., Roepstorff, P., Burchell, J. M., Taylor-Papadimitriou, J., Hollingsworth, M. A., and Clausen, H. (2002) Functional conservation of subfamilies of putative UDP-N-acetylgalactosamine:polypeptide N-acetylgalactosaminyltransferases in Drosophila, Caenorhabditis elegans, and mammals. One subfamily composed of l(2)35Aa is essential in Drosophila. *J Biol Chem* **277**, 22623-22638
22. Ten Hagen, K. G., Tran, D. T., Gerken, T. A., Stein, D. S., and Zhang, Z. (2003) Functional characterization and expression analysis of members of the UDP-GalNAc:polypeptide N-acetylgalactosaminyltransferase family from Drosophila melanogaster. *J Biol Chem* **278**, 35039-35048
23. Bennett, E. P., Mandel, U., Clausen, H., Gerken, T. A., Fritz, T. A., and Tabak, L. A. (2012) Control of mucin-type O-glycosylation: a classification of the polypeptide GalNAc-transferase gene family. *Glycobiology* **22**, 736-756
24. Tran, D. T., and Ten Hagen, K. G. (2013) Mucin-type O-glycosylation during development. *J Biol Chem* **288**, 6921-6929
25. Revoredo, L., Wang, S., Bennett, E. P., Clausen, H., Moremen, K. W., Jarvis, D. L., Ten Hagen, K. G., Tabak, L. A., and Gerken, T. A. (2016) Mucin-type O-glycosylation is controlled by short- and long-range glycopeptide substrate recognition that varies among members of the polypeptide GalNAc transferase family. *Glycobiology* **26**, 360-376
26. Tian, E., and Ten Hagen, K. G. (2006) Expression of the UDP-GalNAc: polypeptide N-acetylgalactosaminyltransferase family is spatially and temporally regulated during Drosophila development. *Glycobiology* **16**, 83-95

27. Ten Hagen, K. G., and Tran, D. T. (2002) A UDP-GalNAc:polypeptide N-acetylgalactosaminyltransferase is essential for viability in Drosophila melanogaster. *J Biol Chem* **277**, 22616-22622
28. Tian, E., Hoffman, M. P., and Ten Hagen, K. G. (2012) O-glycosylation modulates integrin and FGF signalling by influencing the secretion of basement membrane components. *Nat Commun* **3**, 869
29. Tian, E., Stevens, S. R., Guan, Y., Springer, D. A., Anderson, S. A., Starost, M. F., Patel, V., Ten Hagen, K. G., and Tabak, L. A. (2015) Galnt1 is required for normal heart valve development and cardiac function. *PLoS One* **10**, e0115861
30. Tian, E., and Ten Hagen, K. G. (2007) A UDP-GalNAc:polypeptide N-acetylgalactosaminyltransferase is required for epithelial tube formation. *J Biol Chem* **282**, 606-614
31. Tran, D. T., Zhang, L., Zhang, Y., Tian, E., Earl, L. A., and Ten Hagen, K. G. (2012) Multiple members of the UDP-GalNAc: polypeptide N-acetylgalactosaminyltransferase family are essential for viability in Drosophila. *J Biol Chem* **287**, 5243-5252
32. Zhang, L., Syed, Z. A., van Dijk Hard, I., Lim, J. M., Wells, L., and Ten Hagen, K. G. (2014) O-glycosylation regulates polarized secretion by modulating Tango1 stability. *Proc Natl Acad Sci U S A* **111**, 7296-7301
33. Zhang, L., Tran, D. T., and Ten Hagen, K. G. (2010) An O-glycosyltransferase promotes cell adhesion during development by influencing secretion of an extracellular matrix integrin ligand. *J Biol Chem* **285**, 19491-19501
34. Zhang, L., Turner, B., Ribbeck, K., and Ten Hagen, K. G. (2017) Loss of the mucosal barrier alters the progenitor cell niche via Janus kinase/signal transducer and activator of transcription (JAK/STAT) signaling. *J Biol Chem* **292**, 21231-21242
35. Topaz, O., Shurman, D. L., Bergman, R., Indelman, M., Ratajczak, P., Mizrachi, M., Khamaysi, Z., Behar, D., Petronius, D., Friedman, V., Zelikovic, I., Raimer, S., Metzker, A., Richard, G., and Sprecher, E. (2004) Mutations in GALNT3, encoding a protein involved in O-linked glycosylation, cause familial tumoral calcinosis. *Nat Genet* **36**, 579-581
36. Ichikawa, S., Sorenson, A. H., Austin, A. M., Mackenzie, D. S., Fritz, T. A., Moh, A., Hui, S. L., and Econs, M. J. (2009) Ablation of the Galnt3 gene leads to low-circulating intact fibroblast growth factor 23 (Fgf23) concentrations and hyperphosphatemia despite increased Fgf23 expression. *Endocrinology* **150**, 2543-2550
37. Miyazaki, T., Mori, M., Yoshida, C. A., Ito, C., Yamatoya, K., Moriishi, T., Kawai, Y., Komori, H., Kawane, T., Izumi, S., Toshimori, K., and Komori, T. (2013) Galnt3 deficiency disrupts acrosome formation and leads to oligoasthenoteratozoospermia. *Histochem Cell Biol* **139**, 339-354

38. Zara, J., Hagen, F. K., Ten Hagen, K. G., Van Wuyckhuyse, B. C., and Tabak, L. A. (1996) Cloning and expression of mouse UDP-GalNAc:polypeptide N-acetylgalactosaminyltransferase-T3. *Biochem Biophys Res Commun* **228**, 38-44
39. Gresik, E. W. (1975) The postnatal development of the sexually dimorphic duct system and of amylase activity in the submandibular glands of mice. *Cell Tissue Res* **157**, 411-422
40. Tabak, L. A. (1995) In defense of the oral cavity: structure, biosynthesis, and function of salivary mucins. *Annual review of physiology* **57**, 547-564
41. Abusleme, L., Hong, B. Y., Hoare, A., Konkel, J. E., Diaz, P. I., and Moutsopoulos, N. M. (2017) Oral Microbiome Characterization in Murine Models. *Bio Protoc* **7**
42. Zhou, Y., Gao, H., Mihindukulasuriya, K. A., La Rosa, P. S., Wylie, K. M., Vishnivetskaya, T., Podar, M., Warner, B., Tarr, P. I., Nelson, D. E., Fortenberry, J. D., Holland, M. J., Burr, S. E., Shannon, W. D., Sodergren, E., and Weinstock, G. M. (2013) Biogeography of the ecosystems of the healthy human body. *Genome Biol* **14**, R1
43. Geisler, C., and Jarvis, D. L. (2011) Effective glycoanalysis with Maackia amurensis lectins requires a clear understanding of their binding specificities. *Glycobiology* **21**, 988-993
44. Cross, B. W., and Ruhl, S. (2018) Glycan recognition at the saliva - oral microbiome interface. *Cell Immunol* **333**, 19-33
45. Denny, P. A., and Denny, P. C. (1982) Localization of a mouse submandibular sialomucin by indirect immunofluorescence. *Histochem J* **14**, 403-408
46. Denny, P. A., Denny, P. C., and Jenkins, K. (1980) Purification and biochemical characterization of a mouse submandibular sialomucin. *Carbohydr Res* **87**, 265-274
47. Gerken, T. A., Jamison, O., Perrine, C. L., Collette, J. C., Moinova, H., Ravi, L., Markowitz, S. D., Shen, W., Patel, H., and Tabak, L. A. (2011) Emerging paradigms for the initiation of mucin-type protein O-glycosylation by the polypeptide GalNAc transferase family of glycosyltransferases. *J Biol Chem* **286**, 14493-14507
48. Hoare, A., Marsh, P. D., and Diaz, P. I. (2017) Ecological Therapeutic Opportunities for Oral Diseases. *Microbiol Spectr* **5**
49. Rosier, B. T., Marsh, P. D., and Mira, A. (2018) Resilience of the Oral Microbiota in Health: Mechanisms That Prevent Dysbiosis. *J Dent Res* **97**, 371-380
50. Abusleme, L., Diaz, P. I., Freeman, A. F., Greenwell-Wild, T., Brenchley, L., Desai, J. V., Ng, W. I., Holland, S. M., Lionakis, M. S., Segre, J. A., Kong, H. H., and Moutsopoulos, N. M. (2018) Human defects in STAT3 promote oral mucosal fungal and bacterial dysbiosis. *JCI Insight* **3**
51. Moutsopoulos, N. M., Chalmers, N. I., Barb, J. J., Abusleme, L., Greenwell-Wild, T., Dutzan, N., Paster, B. J., Munson, P. J., Fine, D. H., Uzel, G., and Holland, S. M. (2015) Subgingival microbial communities in Leukocyte Adhesion Deficiency and their relationship with local immunopathology. *PLoS Pathog* **11**, e1004698

52. Kiessling, L. L., and Grim, J. C. (2013) Glycopolymer probes of signal transduction. *Chem Soc Rev* **42**, 4476-4491
53. Skoog, E. C., Sjoling, A., Navabi, N., Holgersson, J., Lundin, S. B., and Linden, S. K. (2012) Human gastric mucins differently regulate Helicobacter pylori proliferation, gene expression and interactions with host cells. *PLoS One* **7**, e36378
54. Heo, S. M., Choi, K. S., Kazim, L. A., Reddy, M. S., Haase, E. M., Scannapieco, F. A., and Ruhl, S. (2013) Host defense proteins derived from human saliva bind to Staphylococcus aureus. *Infect Immun* **81**, 1364-1373
55. Ligtenberg, A. J., Walgreen-Weterings, E., Veerman, E. C., de Soet, J. J., de Graaff, J., and Amerongen, A. V. (1992) Influence of saliva on aggregation and adherence of Streptococcus gordonii HG 222. *Infect Immun* **60**, 3878-3884
56. Moshier, A., Reddy, M. S., and Scannapieco, F. A. (1996) Role of type 1 fimbriae in the adhesion of Escherichia coli to salivary mucin and secretory immunoglobulin A. *Curr Microbiol* **33**, 200-208
57. Narimatsu, Y., Joshi, H. J., Nason, R., Van Coillie, J., Karlsson, R., Sun, L., Ye, Z., Chen, Y. H., Schjoldager, K. T., Steentoft, C., Furukawa, S., Bensing, B. A., Sullam, P. M., Thompson, A. J., Paulson, J. C., Bull, C., Adema, G. J., Mandel, U., Hansen, L., Bennett, E. P., Varki, A., Vakhrushev, S. Y., Yang, Z., and Clausen, H. (2019) An Atlas of Human Glycosylation Pathways Enables Display of the Human Glycome by Gene Engineered Cells. *Mol Cell* **75**, 394-407 e395
58. Romanenko, V. G., Nakamoto, T., Srivastava, A., Begenisich, T., and Melvin, J. E. (2007) Regulation of membrane potential and fluid secretion by Ca2+-activated K+ channels in mouse submandibular glands. *J Physiol* **581**, 801-817
59. Caporaso, J. G., Lauber, C. L., Walters, W. A., Berg-Lyons, D., Lozupone, C. A., Turnbaugh, P. J., Fierer, N., and Knight, R. (2011) Global patterns of 16S rRNA diversity at a depth of millions of sequences per sample. *Proc Natl Acad Sci U S A* **108 Suppl 1**, 4516-4522
60. Schloss, P. D., Westcott, S. L., Ryabin, T., Hall, J. R., Hartmann, M., Hollister, E. B., Lesniewski, R. A., Oakley, B. B., Parks, D. H., Robinson, C. J., Sahl, J. W., Stres, B., Thallinger, G. G., Van Horn, D. J., and Weber, C. F. (2009) Introducing mothur: open-source, platform-independent, community-supported software for describing and comparing microbial communities. *Appl Environ Microbiol* **75**, 7537-7541
61. Kozich, J. J., Westcott, S. L., Baxter, N. T., Highlander, S. K., and Schloss, P. D. (2013) Development of a dual-index sequencing strategy and curation pipeline for analyzing amplicon sequence data on the MiSeq Illumina sequencing platform. *Appl Environ Microbiol* **79**, 5112-5120
62. Segata, N., Izard, J., Waldron, L., Gevers, D., Miropolsky, L., Garrett, W. S., and Huttenhower, C. (2011) Metagenomic biomarker discovery and explanation. *Genome Biol* **12**, R60

Abbreviations

The abbreviations used are: Galnt, UDP-GalNAc:polypeptide N-acetylgalactosaminyltransferases; Gal, galactose; GalNAc, N-acetylgalactosamine; PNA, peanut agglutinin; SMG, submandibular gland; MAA, *Maackia amurensis* agglutinin; OUT, operational taxonomic units; HFTC, hyperphosphatemic familial tumoral calcinosis; NM, neuraminidase.

Figures legends

Fig. 1. *Galnt3* is the most abundantly expressed isoform in adult SMGs. (A) Expression of *Galnt* family members in embryonic SMGs detected by qPCR. *Galnt1* is the predominant isoform at E13, and *Galnt2* is the predominant isoform at E15 and E17. **(B)** Expression of *Galnt* family members (with greater than 2% relative expression) in early postnatal and adult SMGs. Expression of entire murine *Galnt* family is shown in supplementary Figure S1A. *Galnt3* is the most abundant isoform in adult SMGs. Values represent mean ± SD from three or more animals. Expression was normalized to *29S* rRNA and is represented as percentage of total *Galnt* expression for each individual stage of development. **(C)** *In situ* hybridization using tyramide signal amplification (TSA) in combination with immunofluorescent staining of 8 wk SMGs shows that *Galnt3* mRNA (red) is found specifically in acinar cells (detected by Aqp5, cyan) in both males and females. Nuclear staining is shown in blue. Scale bar, 10 μm.

Fig. 2. Loss of *Galnt3* alters the oral microbiome. Principle coordinates analysis (PCoA) plots of oral swab samples based on θ YC distances (to analyze microbial community structure) with 95% confidence ellipses. The oral microbiome was sampled at both 8 wks and 12 wks for each individual animal. For both 8 wk **(A)** and 12 wk old **(B)** males, *WT* samples (red dots) cluster apart from *Galnt3*$^{-/-}$ samples (gray dots). Each dot represents an individual mouse. At both 8 wks and 12 wks of age, statistically significant differences between *WT* and *Galnt3*$^{-/-}$ samples were determined by AMOVA ($p < 0.05$). For females, no significant differences between *WT* (brown dots) and *Galnt3*$^{-/-}$ (pink dots) samples were observed at 8 wks **(C)** or 12 wks of age **(D)**. Relative abundance of bacterial taxa at genus level in oral swab samples from 8 wk **(E)** and 12 wk old **(F)** males. Each bar represents one mouse. Unclassified genera are shown at family level. Species level taxonomy is reported in parenthesis when > 97% similarity was achieved using NCBI BLAST. * indicates species over-represented in *WT* samples and # represents species over-represented in *Galnt3*$^{-/-}$ samples according to LEfSe analyses.

Fig. 3. Loss of *Galnt3* alters stability of the oral microbiome over time. Principle coordinates analysis (PCoA) plots comparing 8 wk and 12 wk oral swab samples based on θ YC distances (to analyze microbial community structure) with 95% confidence ellipses. The oral microbiome was sampled at both 8 wks and 12 wks for each individual animal. For both *WT* males **(A)** and females **(B)**, no significant differences between 8 wk and 12 wk samples were observed. For *Galnt3*$^{-/-}$ animals, 8 wk samples cluster apart from 12 wk samples for both males **(C)** and females **(D)**. Statistically significant differences between 8 wk and 12 wk *Galnt3*$^{-/-}$ samples were determined by AMOVA ($p < 0.05$). Relative abundance of bacterial taxa at genus

level in oral swab samples from male **(E)** and female **(F)** *Galnt3*$^{-/-}$ animals. Each bar represents one mouse. Unclassified genera are shown at family level. Species level taxonomy is reported in parenthesis when > 97% similarity was achieved using NCBI BLAST. * indicates species over-represented in 12 wk samples and # represents species over-represented in 8 wk samples according to LEfSe analyses.

Fig. 4. Glycans present within the acinar cells of SMGs. Immunofluorescent staining of 8 wk *WT* female **(A)** and male **(B)** SMGs with the lectin MAA (green), which detects α2,3 linked sialic acid on O- and N-linked glycans. Samples were either untreated (no NM) or treated with neuraminidase (NM), which removes sialic acid to show specificity. Acinar cells are shown with the marker Acinar-1 (red). Nuclei are shown in blue. Scale bars, 20 μm. Immunofluorescent staining of 8 wk *WT* female **(C)** and male **(D)** SMGs with the lectin PNA (green), which detects the non-sialylated core 1 O-glycan Galβ1,3GalNAc. Samples were either untreated (no NM) or treated with neuraminidase (NM). No PNA staining is seen in untreated female SMGs whereas PNA staining is seen in both treated and untreated male SMGs. Acinar cells are shown with the marker Acinar-1 (red). Nuclei are shown in blue. Scale bars, 10 μm. Western blots of *WT* female **(E)** and male **(F)** SMG extracts either untreated (-) or treated with NM (+) and probed with PNA. Molecular weight markers (kDa) are shown to the left of each blot.

Fig. 5. Loss of *Galnt3* results in diminished O-glycans in male acinar cells. Immunofluorescent staining of 8 wk *WT* and *Galnt3*$^{-/-}$ male **(A)** and female **(B)** SMGs with the lectin MAA (green), which detects α2,3 linked sialic acid on O- and N-linked glycans. Acinar cells are shown with the marker Acinar-1 (red). Nuclei are shown in blue. Scale bars, 10 μm. **(C)** Immunofluorescent staining of 8 wk male SMGs shows a dramatic reduction in O-glycans (detected by PNA, red) specifically in the acinar cells (detected by Acinar-1, cyan) of *Galnt3*$^{-/-}$ SMGs as compared to *WT*. **(D)** Immunofluorescent staining of neuraminidase-treated 8 wk female SMGs reveals no obvious differences in PNA-reactive O-glycans between *WT* and *Galnt3*$^{-/-}$ SMGs. Nuclear staining is shown in blue. Scale bars, 20 μm.

Fig. 6. Analysis of *mucin* gene expression in early postnatal and adult SMGs. (A) qPCR analysis demonstrates that *Muc10* is the most abundantly expressed mucin gene at all five stages, with increasing expression in adult stages. Moderate to low levels of expression were detected for *Muc13* **(B)**, *Muc20* **(C)**, and *Muc1* **(D).** *Muc2*, *Muc4*, *Muc5ac*, and *Muc6* were not detected at any stage. Values represent mean ± SD from three or more animals. Expression was normalized to *29S* rRNA. **(E)** Immunofluorescent staining of 8 wk SMGs shows specific localization of Muc10 protein (red) to acinar cells (detected by Acinar-1, cyan) in both males and females. Nuclear staining is shown in blue. Scale bar, 20 μm.

Fig. 7. Muc10 is an in vivo substrate for Galnt3. (A) Western blots of 8 wk male SMG lysates probed for O-glycans (detected by PNA, red) and Muc10 (green). Separated channels are shown in black in the top two panels and merged channels are shown in color in the bottom panel. The lower of the two PNA-reactive bands overlaps with the Muc10 band in *WT* SMGs. In *Galnt3*$^{-/-}$ SMGs, the lower PNA-reactive band is absent and the Muc10 band is smeared and reduced in size. **(B)** Western blots of neuraminidase-treated 8

wk female SMG lysates probed for O-glycans (detected by PNA, red) and Muc10 (green). The PNA and Muc10 bands overlap in both *WT* and *Galnt3*$^{-/-}$ SMGs. In *Galnt3*$^{-/-}$ SMGs, both the PNA and Muc10 bands exhibit altered mobility as compared to *WT*. Molecular weight markers (kDa) are shown to the left of each blot. **(C)** In vitro enzymatic activity of Galnt3 against Muc10 acceptor peptides (peptide sequences shown in **(D)**). EA2 was used as a positive control. Galnt3 was able to glycosylate the Muc10-s, Muc10-273, Muc10-264, and Muc10-l peptides. Galnt3 showed no activity toward the Muc10-10 peptide. Each data point represents an individual assay. Error bars are SD.

Figure 1

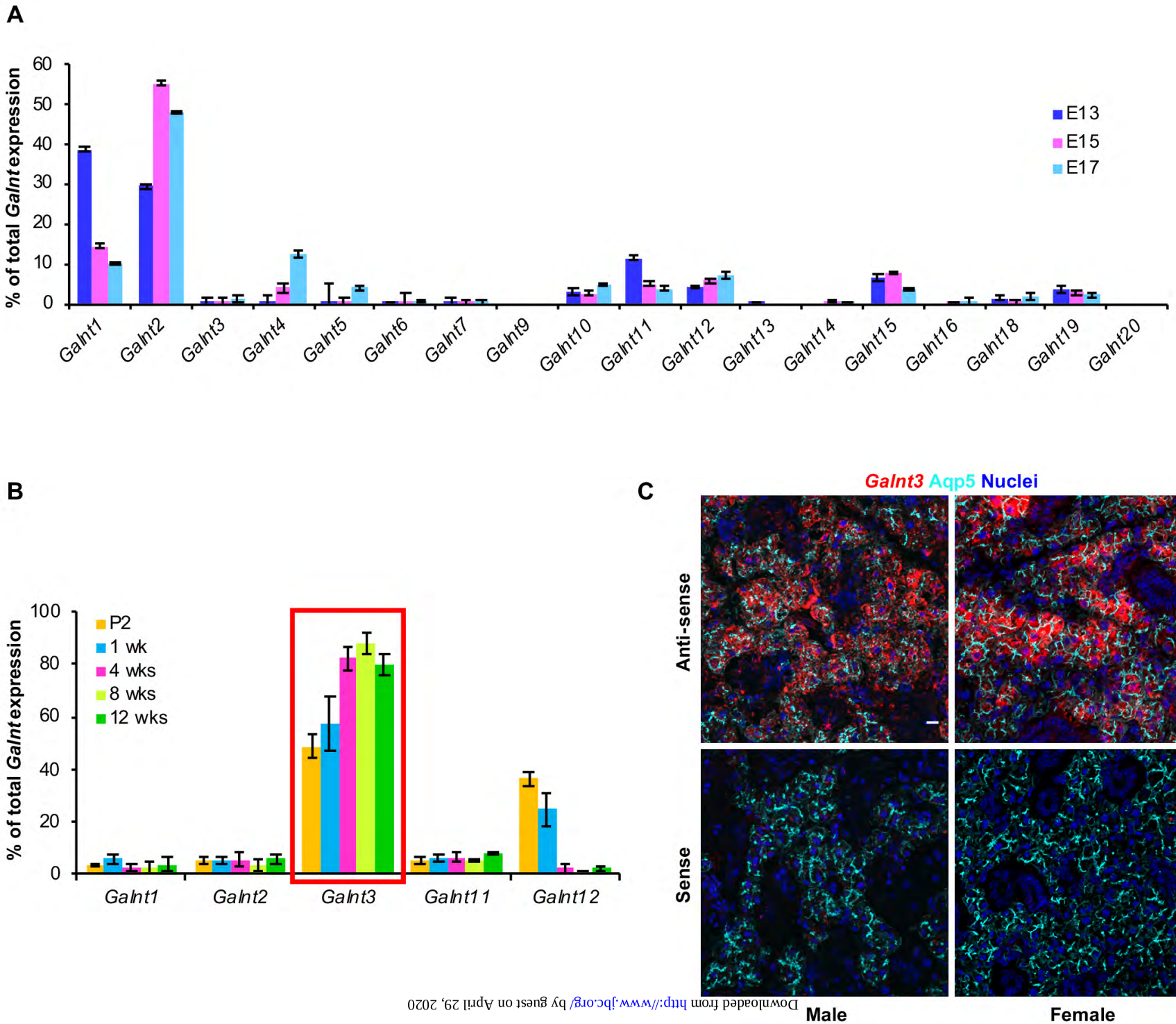

Figure 2

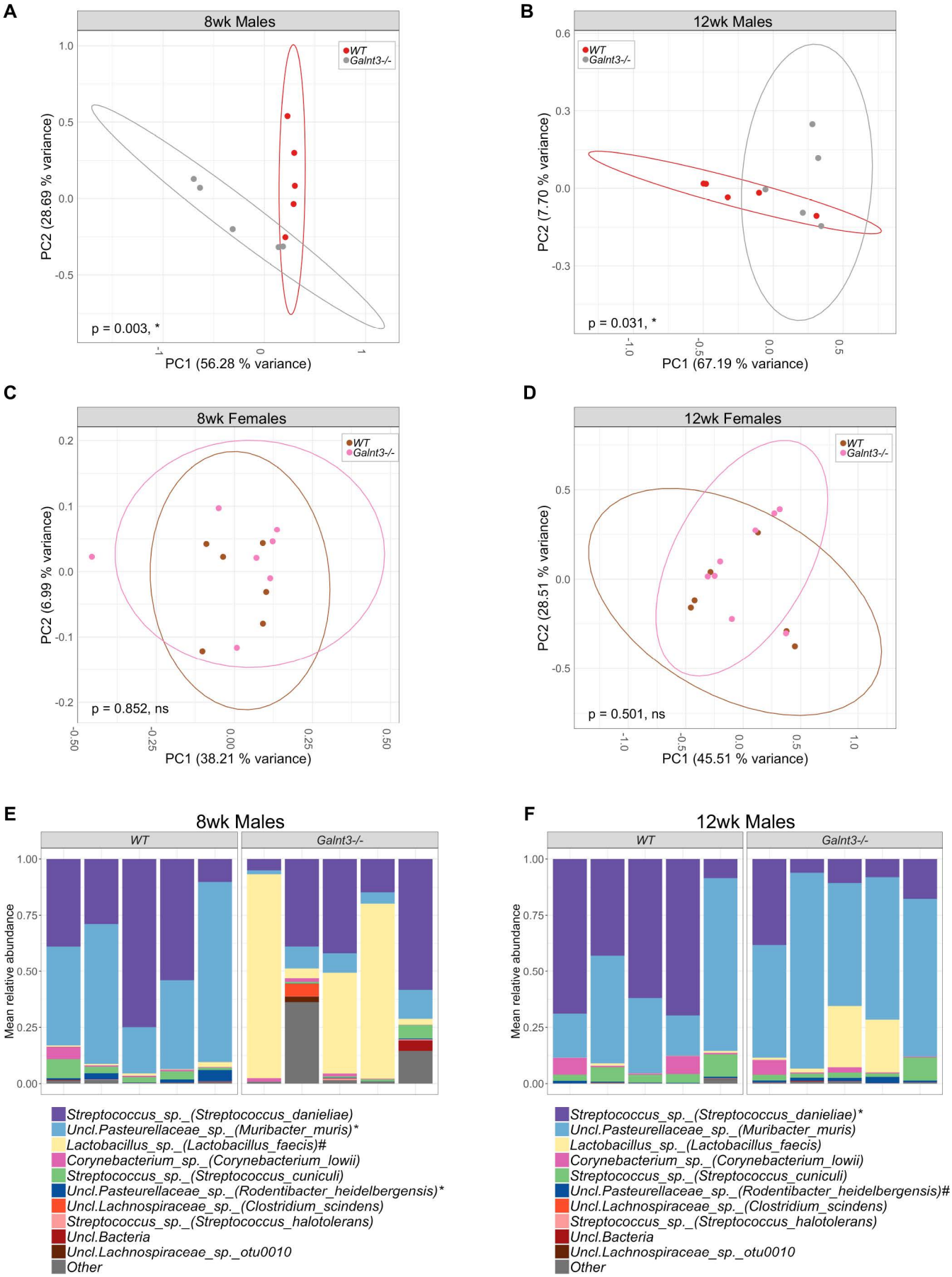
A
8wk Males
WT
Galnt3-/-
PC2 (28.69 % variance)
PC1 (56.28 % variance)
p = 0.003, *
B
12wk Males
PC2 (7.70 % variance)
PC1 (67.19 % variance)
p = 0.031, *
C
8wk Females
PC2 (6.99 % variance)
PC1 (38.21 % variance)
p = 0.852, ns
D
12wk Females
PC2 (28.51 % variance)
PC1 (45.51 % variance)
p = 0.501, ns
E
8wk Males
WT
Galnt3-/-
Mean relative abundance
Streptococcus_sp._(Streptococcus_danieliae)
Uncl.Pasteurellaceae_sp._(Muribacter_muris)*
Lactobacillus_sp._(Lactobacillus_faecis)#
Corynebacterium_sp._(Corynebacterium_lowii)
Streptococcus_sp._(Streptococcus_cuniculi)
Uncl.Pasteurellaceae_sp._(Rodentibacter_heidelbergensis)*
Uncl.Lachnospiraceae_sp._(Clostridium_scindens)
Streptococcus_sp._(Streptococcus_halotolerans)
Uncl.Bacteria
Uncl.Lachnospiraceae_sp._otu0010
Other
F
12wk Males
WT
Galnt3-/-
Mean relative abundance
Streptococcus_sp._(Streptococcus_danieliae)*
Uncl.Pasteurellaceae_sp._(Muribacter_muris)
Lactobacillus_sp._(Lactobacillus_faecis)
Corynebacterium_sp._(Corynebacterium_lowii)
Streptococcus_sp._(Streptococcus_cuniculi)
Uncl.Pasteurellaceae_sp._(Rodentibacter_heidelbergensis)#
Uncl.Lachnospiraceae_sp._(Clostridium_scindens)
Streptococcus_sp._(Streptococcus_halotolerans)
Uncl.Bacteria
Uncl.Lachnospiraceae_sp._otu0010
Other

Figure 3

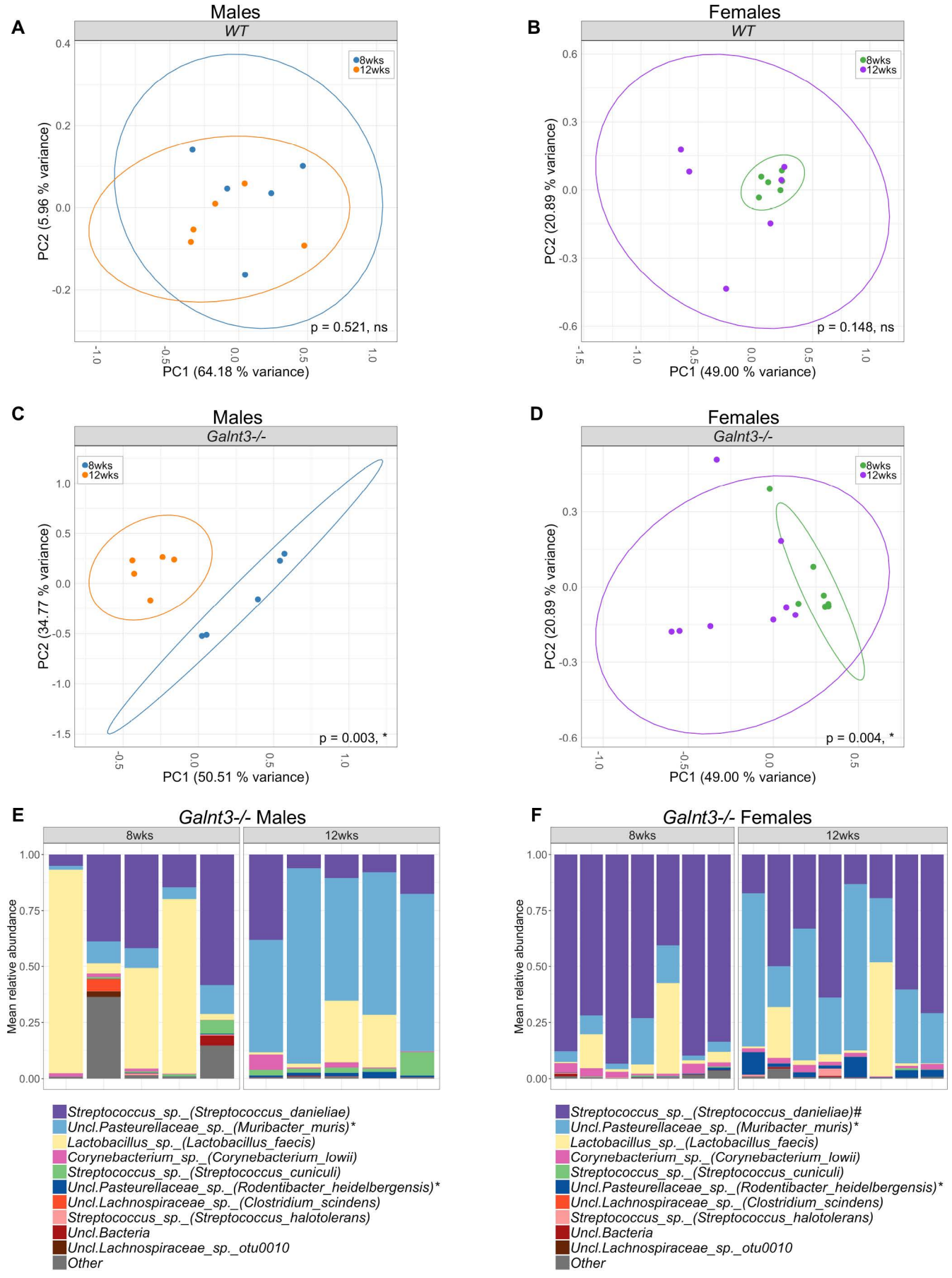
A
Males
WT
8wks
12wks
PC2 (5.96 % variance)
PC1 (64.18 % variance)
p = 0.521, ns
B
Females
WT
8wks
12wks
PC2 (20.89 % variance)
PC1 (49.00 % variance)
p = 0.148, ns
C
Males
Galnt3-/-
8wks
12wks
PC2 (34.77 % variance)
PC1 (50.51 % variance)
p = 0.003, *
D
Females
Galnt3-/-
8wks
12wks
PC2 (20.89 % variance)
PC1 (49.00 % variance)
p = 0.004, *
E
Galnt3-/- Males
8wks
12wks
Mean relative abundance
F
Galnt3-/- Females
8wks
12wks
Mean relative abundance
Streptococcus_sp._(Streptococcus_danieliae)
Uncl.Pasteurellaceae_sp._(Muribacter_muris)*
Lactobacillus_sp._(Lactobacillus_faecis)
Corynebacterium_sp._(Corynebacterium_lowii)
Streptococcus_sp._(Streptococcus_cuniculi)
Uncl.Pasteurellaceae_sp._(Rodentibacter_heidelbergensis)*
Uncl.Lachnospiraceae_sp._(Clostridium_scindens)
Streptococcus_sp._(Streptococcus_halotolerans)
Uncl.Bacteria
Uncl.Lachnospiraceae_sp._otu0010
Other
Streptococcus_sp._(Streptococcus_danieliae)#
Uncl.Pasteurellaceae_sp._(Muribacter_muris)*
Lactobacillus_sp._(Lactobacillus_faecis)
Corynebacterium_sp._(Corynebacterium_lowii)
Streptococcus_sp._(Streptococcus_cuniculi)
Uncl.Pasteurellaceae_sp._(Rodentibacter_heidelbergensis)*
Uncl.Lachnospiraceae_sp._(Clostridium_scindens)
Streptococcus_sp._(Streptococcus_halotolerans)
Uncl.Bacteria
Uncl.Lachnospiraceae_sp._otu0010
Other

Figure 4

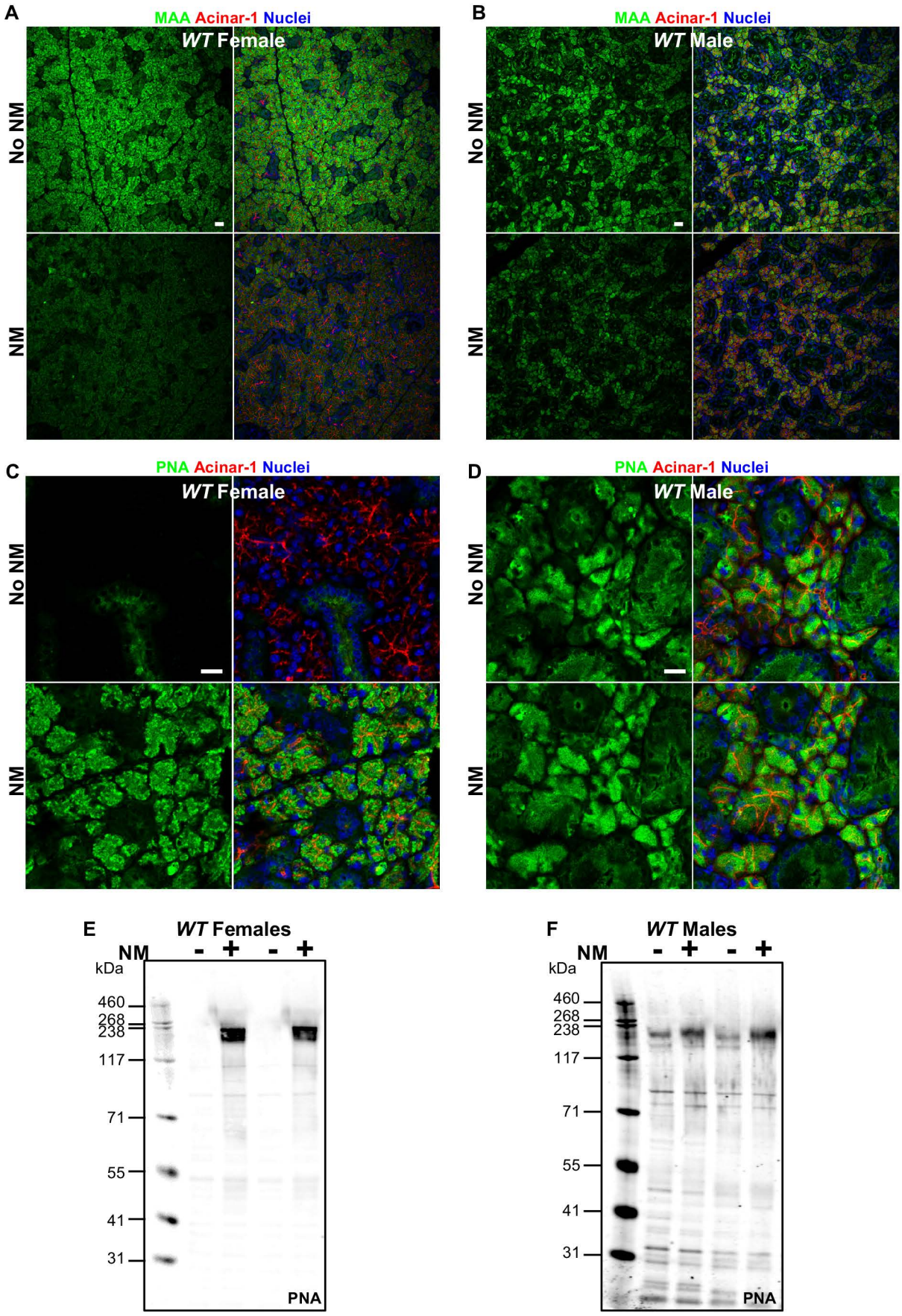
A
MAA Acinar-1 Nuclei
WT Female
No NM
NM
B
MAA Acinar-1 Nuclei
WT Male
No NM
NM
C
PNA Acinar-1 Nuclei
WT Female
No NM
NM
D
PNA Acinar-1 Nuclei
WT Male
No NM
NM
E
WT Females
NM - + - +
kDa
460
268
238
117
71
55
41
31
PNA
F
WT Males
NM - + - +
kDa
460
268
238
117
71
55
41
31
PNA

Figure 5

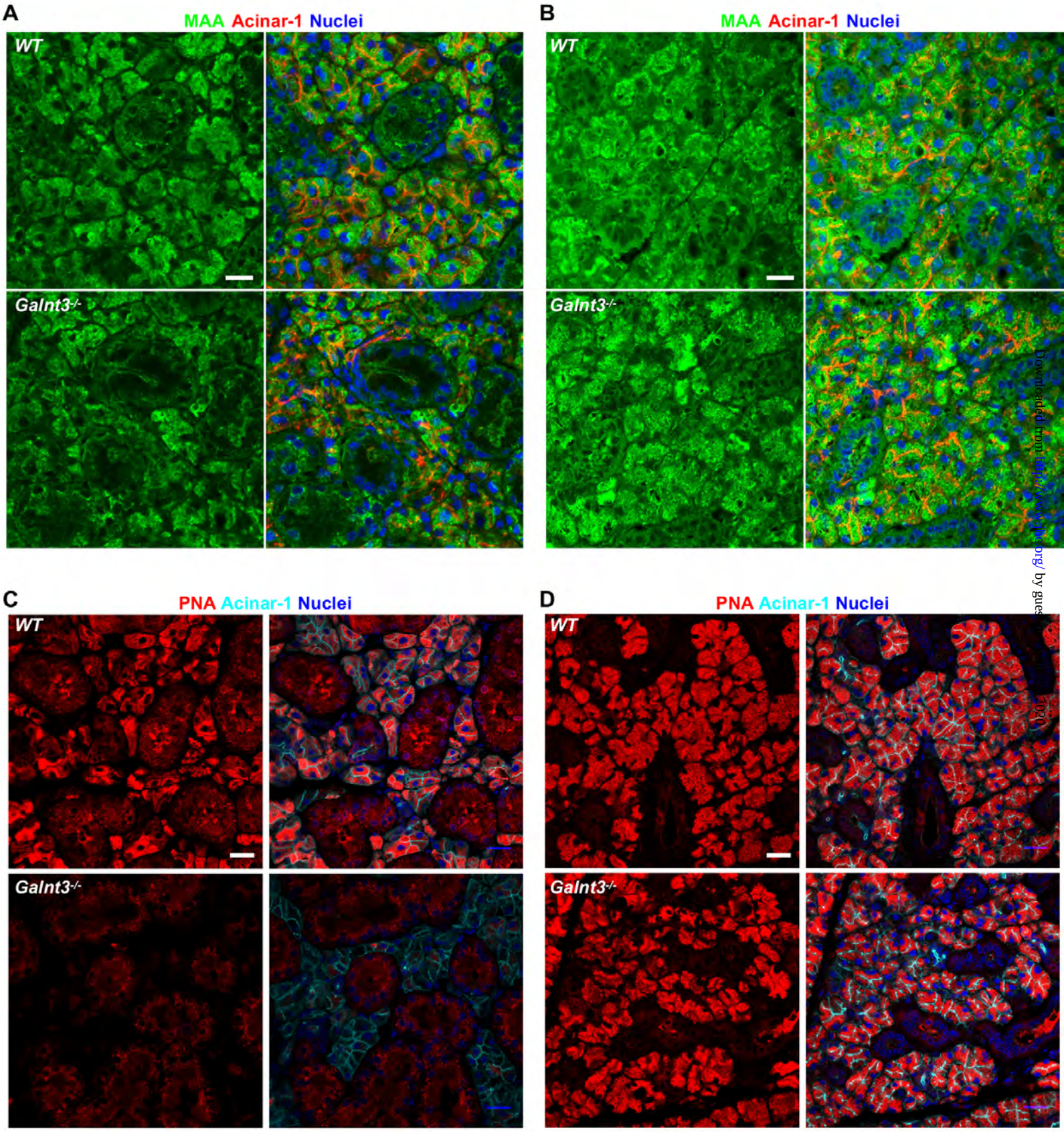

Figure 6

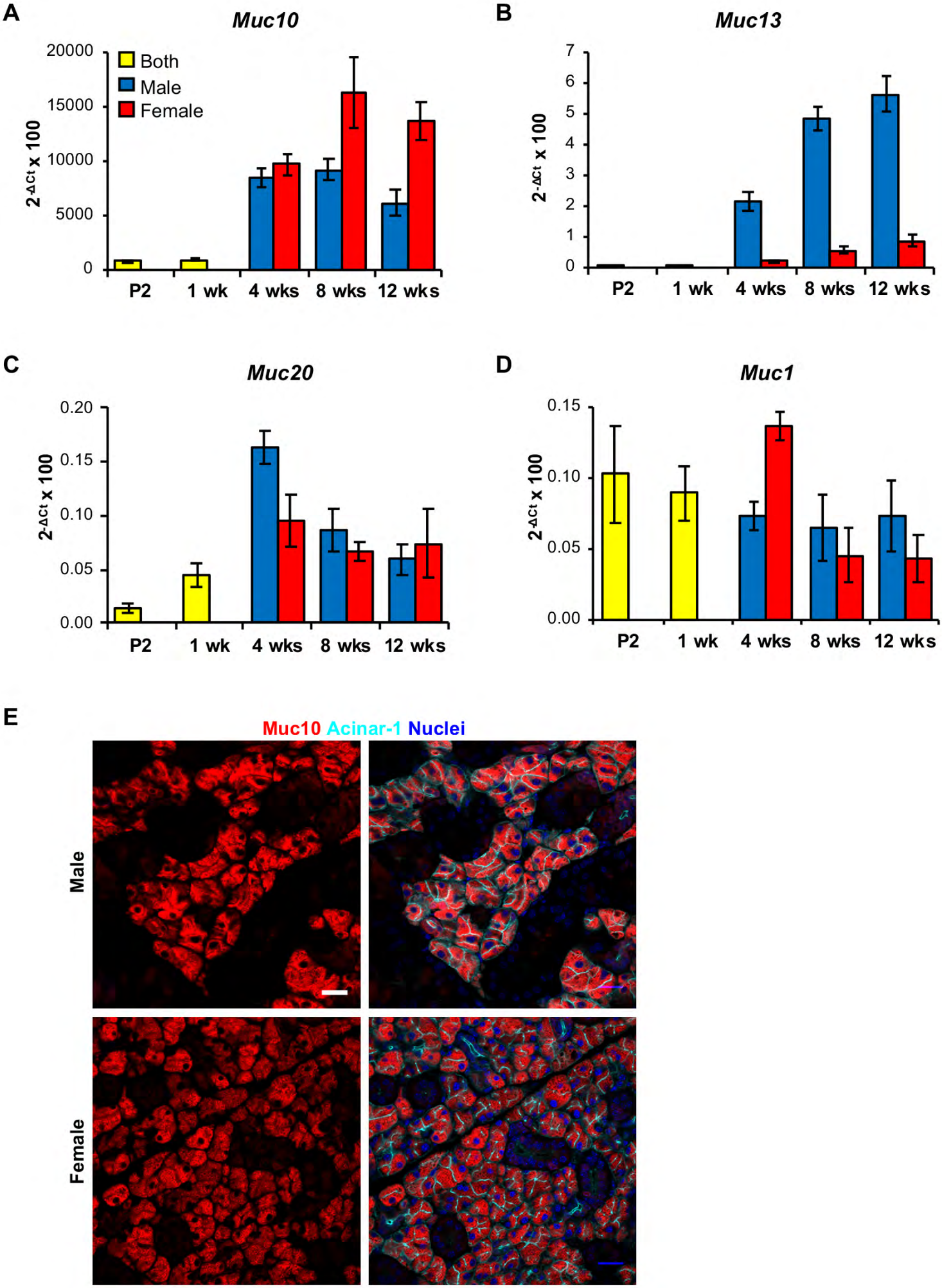

Figure 7

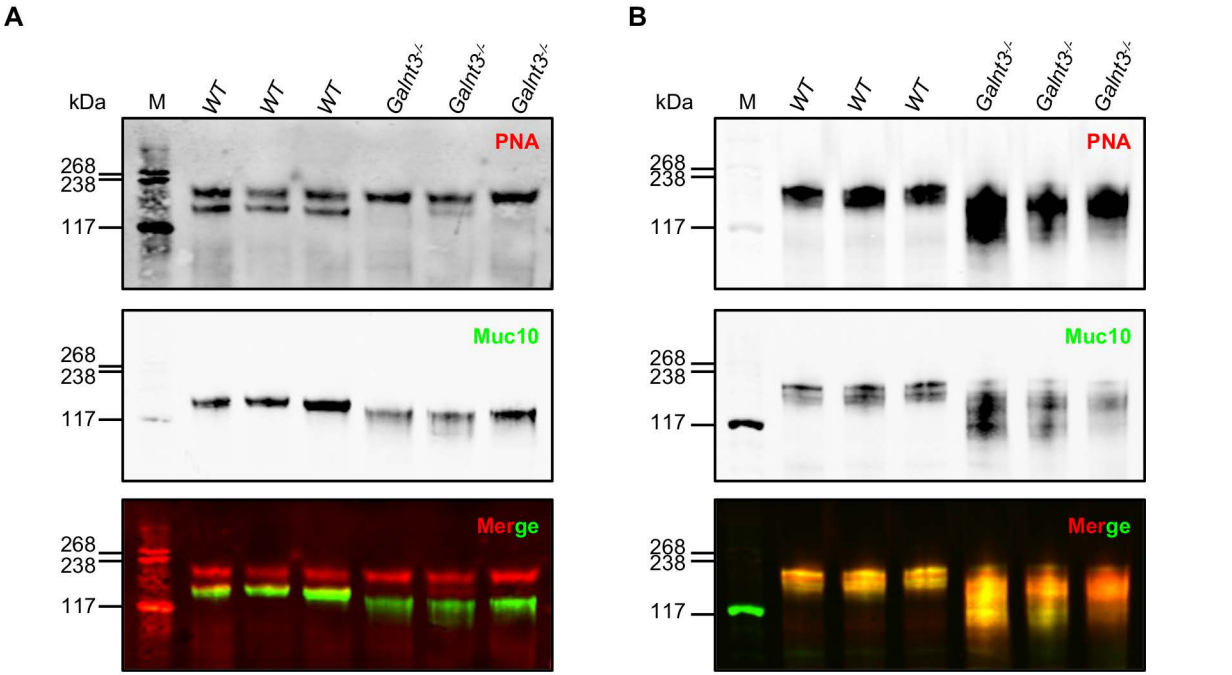

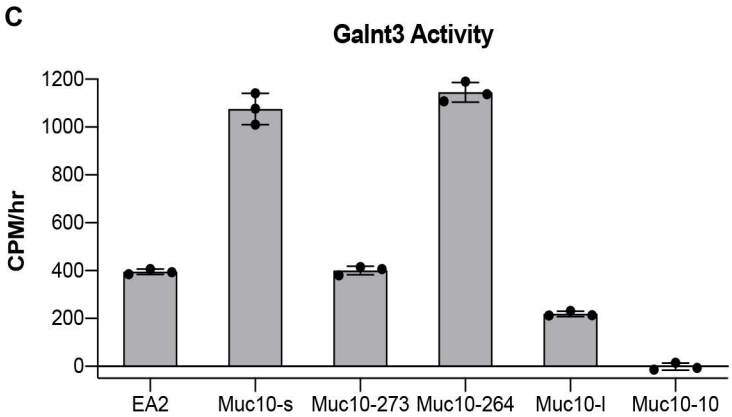

D

Peptide	Sequence
EA2	PTTDSTTPAPTTK
Muc10-s	NATTPAPTLK
Muc10-273	NRTTTNATTPAPTTK
Muc10-264	NRTTTNAITPAPTPK
Muc10-l	NATTPATTTNATTPATTTK
Muc10-10	ANSTSSTTTSTTIQ

Loss of the disease-associated glycosyltransferase Galnt3 alters Muc10 glycosylation and the composition of the oral microbiome

Gabriella Peluso, E Tian, Loreto Abusleme, Takashi Munemasa, Taro Mukaibo and Kelly G. Ten Hagen

J. Biol. Chem. published online December 27, 2019
